Quadricyclane Radical Cation Rearrangements: A Computational Study of the Transformations to 1,3,5-Cycloheptatriene and Norbornadiene

Per-Erik Larsson, Nessima Salhi-Benachenhou,* and Sten Lunell[a]

Dedicated to Professor Osvaldo Goscinski on the occasion of his 65th birthday

Abstract: An alternative skeletal rearrangement of the quadricyclane radical cation ($\mathbf{Q}^{\cdot+}$) explains the side products formed in the one-electron oxidation to norbornadiene. First, the bicyclo[2.2.1]hepta-2-ene-5-yl-7-ylium radical cation, with an activation energy of 14.9 kcal mol^{-1}, is formed. Second, this species can further rearrange to 1,3,5-cycloheptatriene through two plausible paths, that is, a multistep mechanism with two shallow intermediates and a stepwise path in which the bicyclo[3.2.0]hepta-2,6-diene radical cation is an intermediate. The multistep rearrangement has a rate-limiting step with an estimated activation energy of 16.5 kcal mol^{-1}, which is 2.8 kcal mol^{-1} lower in energy than the stepwise mechanism. However, the lowest activation energy is found for the $\mathbf{Q}^{\cdot+}$ cycloreversion to norbornadiene that has a transition structure, in close correspondence with earlier studies, and an activation energy of 10.1 kcal mol^{-1}, which agrees well with the experimental estimate of 9.3 kcal mol^{-1}. The computational estimates of activation energies were done using the CCSD(T)/6–311+G(d,p) method with geometries optimized on the B3LYP/6–311+G(d,p) level, combined with B3LYP/6–311+G(d,p) frequencies.

Keywords: density functional calculations · electronic structure · EPR spectroscopy · radical ions · rearrangement

Introduction

Hydrocarbon radical cations are becoming increasingly important as reactive intermediates in chemistry. This is reflected, for example, in the increased use of one-electron oxidations in organic chemistry and may lead to enormous rate accelerations.[1] Yet, the understanding of electronic structure and stability is still rather limited for these reactive species. The major reason for this is the fast rearrangement or fragmentation that makes experimental measurements difficult. An unexpected rearrangement can also lead to novel structures, not present in the closed-shell equivalent, that potentially can produce novel chemical transformations.

In the isomerization reactions of quadricyclanes, a facile conversion from the quadricyclane radical cation ($\mathbf{Q}^{\cdot+}$) to the norbornadiene radical cation ($\mathbf{N}^{\cdot+}$) has become a prototype for one-electron oxidation reactions. Because of its extremely facile conversion the **Q**/**N** system has been suggested as a potential solar-energy storage system.[2] Actually, it was not until 1994 that a direct observation of $\mathbf{Q}^{\cdot+}$ was reported by using electron spin resonance (ESR) spectroscopy.[3,4] The signal disappears after ~1.5 μs at room temperature;[3] all prior experimental studies gave only indications of its existence[5] or was characterized as $\mathbf{N}^{\cdot+}$. The computational studies performed on this cycloreversion agree with the experimental observations that $\mathbf{Q}^{\cdot+}$ is an unstable species. Moreover, it is found that the cycloreversion takes place through a concerted mechanism with a pseudo-Jahn–Teller distorted transition structure and an estimated activation energy in the range 5–12 kcal mol^{-1}.[6]

However, in several studies, additional radical cation species have been observed when starting from $\mathbf{Q}^{\cdot+}$.[4,7–10] From ESR studies in a CF_3CCl_3 matrix it was concluded that these additional species were the bicyclo[3.2.0]hepta-2,6-diene ($\mathbf{BHD}^{\cdot+}$) and the 1,3,5-cycloheptatriene ($\mathbf{CHT}^{\cdot+}$) radical cations.[7] The ^{1}H hyperfine coupling constants (hfcc) were later confirmed by ESR measurements in zeolites, and the conversion was measured to always be less than 3% of concentration.[4,8] Interestingly, if **Q** is substituted with isopropylidene the one-electron oxidation reaction gives only **BHD** as product, in quantitative yield.[11] In a recent computational study, we investigated the mechanism for this alternative rearrangement and found that it follows a stepwise rearrangement path with an intermediate—the bicyclo[2.2.1]hepta-2-ene-5-yl-7-ylium radical cation ($\mathbf{BHE}^{\cdot+}$)—

[a] Dr. P.-E. Larsson, Dr. N. Salhi-Benachenhou, Prof. S. Lunell
Department of Quantum Chemistry
Uppsala University, Box 518, 751 20 Uppsala (Sweden)
Fax: (+46) 18-471-5830
E-mail: Nessima.Salhi@kvac.uu.se

Supporting information for this article is available on the WWW under http://www.chemeurj.org/ or from the author.

 DOI: 10.1002/chem.200305067 © 2004 Wiley-VCH Verlag GmbH & Co. KGaA, Weinheim

that is ~2.5 kcal mol^{-1} more stable than **BHD**$^{\cdot+}$ for CCSD(T)/6–311+G(d,p)//B3LYP/6–311+G(d,p) calculations.[12] Moreover, we found that the hfcc previously assigned to **BHD**$^{\cdot+}$ agree much better with **BHE**$^{\cdot+}$. Thus, we concluded that the two rearrangements paths **Q**$^{\cdot+}$ can take is to the major product **N**$^{\cdot+}$ and to the alternative rearrangement that produces **BHE**$^{\cdot+}$ (Scheme 1).

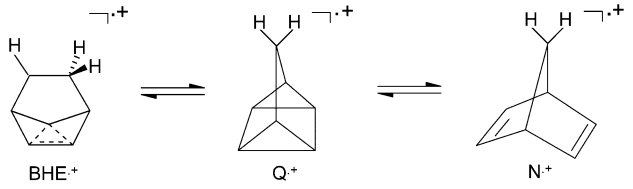

Scheme 1. Rearrangement channels from **Q**$^{\cdot+}$.

This other $C_7H_8^{\cdot+}$ rearrangement chemistry has attracted less attention than the **Q**$^{\cdot+}$/**N**$^{\cdot+}$ system, but it could give valuable information of the different side products that can be expected upon substitution and environmental changes. For instance, **CHT**$^{\cdot+}$ is observed together with **BHE**$^{\cdot+}$ and several deprotonated neutral radicals in ESR studies of **Q**$^{\cdot+}$ and **N**$^{\cdot+}$ in different matrices. Moreover, ESR studies of **BHD** in a $CFCl_3$ matrix give, after γ-irradiation, the hfcc assigned to **BHE**$^{\cdot+}$ together with a hfcc assigned to **CHT**$^{\cdot+}$.[13] This observation of **CHT**$^{\cdot+}$ was ascribed to an electrocyclic ring-opening reaction of **BHD**$^{\cdot+}$, but in view of the reinterpretation of the **BHD**$^{\cdot+}$ spectra just described, other rearrangement channels that transform **BHE**$^{\cdot+}$ directly into **CHT**$^{\cdot+}$ should be explored (Scheme 2).

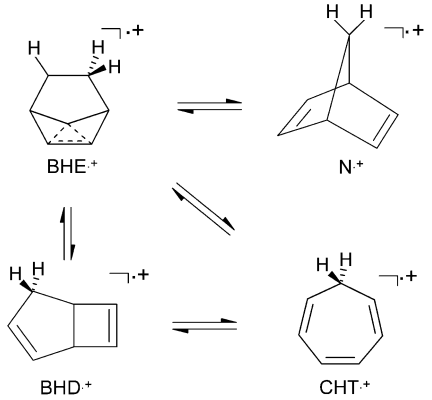

Scheme 2. Rearrangement channels from **BHE**$^{\cdot+}$.

In this paper we report results from a quantum chemical study, including estimations of activation energies, for alternative rearrangements of the $C_7H_8^{\cdot+}$ species **Q**$^{\cdot+}$. In particular, we characterize two reaction paths for how **BHE**$^{\cdot+}$ can rearrange to **CHT**$^{\cdot+}$, that is, a multistep rearrangement with two shallow minima, on the one hand, and a stepwise rearrangement through **BHD**$^{\cdot+}$ with the electrocyclic ring opening, on the other. Furthermore, we also report results for the transformation of **BHE**$^{\cdot+}$ to **N**$^{\cdot+}$ (Scheme 2) and from **Q**$^{\cdot+}$ to **BHE**$^{\cdot+}$ and **N**$^{\cdot+}$, respectively (Scheme 1).

Results and Discussion

The optimized structures from B3LYP/6–311+G(d,p) calculations of the local minima **Q**$^{\cdot+}$, **N**$^{\cdot+}$, **BHE**$^{\cdot+}$, **BHD**$^{\cdot+}$ and **CHT**$^{\cdot+}$ are displayed in Figure 1 with selected atomic distances. A comparison of the geometric parameters obtained from the B3LYP calculations with the MP2/6–311+G(d,p) results shows that these are very similar in most cases. The largest deviation is found for **BHD**$^{\cdot+}$ (C4–C6 distance 0.096 Å, C4-C5-C6 angle 5.46°, and C7-C1-C5-C6 dihedral angle 5.09°), for which the MP2 optimization predicts a more open structure than B3LYP; this may be due to the spin contamination of the MP2 wave function. For **N**$^{\cdot+}$ (C2–C6 distance 0.030 Å and C6-C1-C2 angle 1.24°) B3LYP predicts a more open structure. All other differences are less than 0.013 Å for distances, 0.80° for angles and 0.76° for dihedral angles. That these structures are indeed accurately computed can be confirmed by comparison of the B3LYP hfcc with the experimental ones. Very good agreement is found for the **Q**$^{\cdot+}$, **N**$^{\cdot+}$, **BHE**$^{\cdot+}$, and **CHT**$^{\cdot+}$ structures; see Table 1 for the hfcc values of particular importance for this work.[3,4,7,13,14]

Table 1. ^{1}H hyperfine coupling constants in Gauss for **BHE**$^{\cdot+}$, **BHD**$^{\cdot+}$, and **CHT**$^{\cdot+}$ computed with B3LYP/6–311+G(d,p), and compared to experimental values observed in Freon matrices.

BHE$^{\cdot+}$	**BHD**$^{\cdot+}$	Exptl[a]	**CHT**$^{\cdot+}$	Exptl[a,b]
41.0 (H6a)	25.6 (H2a)	41.5	51.2 (H7a)	51.5
30.7 (H6b)	17.6 (H1)	31.6	51.2 (H7b)	51.5
−22.7 (H5)	16.8 (H2b)	22.5	−6.9 (H1)	5.7
4.9 (H4)	−3.7 (H3)	4.5	−6.9 (H6)	5.7
3.3 (H3)	−3.0 (H4)	4.5	−4.7 (H3)	5.7
0.6 (H2)	−3.0 (H5)	–	−4.7 (H4)	5.7
0.4 (H7)	1.1 (H7)	–	−0.7 (H2)	–
−0.3 (H1)	−0.1 (H6)	–	−0.7 (H5)	–

[a] Reference [7]. [b] Reference [14a].

From the local minima on the $C_7H_8^{\cdot+}$ potential-energy surface we located plausible reaction paths corresponding to Schemes 1 and 2, using the B3LYP/6–31G(d) method. The refined structures for the saddle points and local minima calculated with B3LYP/6–311+G(d,p) are shown in Figures 2 and 3. They show in general larger structural deviations between B3LYP and MP2 than the stationary points in Figure 1; for the **TS4** structure we were not able to locate a MP2 transition structure, probably because of the severe spin contamination in the UMP2 wave function. The largest deviations are for **TS1**, **TS3**, **TS5** and **TS6**, that is, for **TS1** (C3–C5 = 0.042 Å and C3-C5-C6 = 14.86°) the MP2 saddle point on the cycloreversion path are more pseudo-Jahn–Teller distorted away from the C_{2v} conical intersection;[6] for **TS3** (C4–C5 = 0.220 Å, C4-C7-C5 = 11.82° and C6-C1-C7-C4 = 6.85°) the MP2 result indicates a later transition state on the isomerization from **BHE**$^{\cdot+}$ to **BHD**$^{\cdot+}$; for **TS5** (C3–C6 = 0.294 Å, and C4-C5-C6 = 8.06°) B3LYP predicts a later

© 2004 Wiley-VCH Verlag GmbH & Co. KGaA, Weinheim

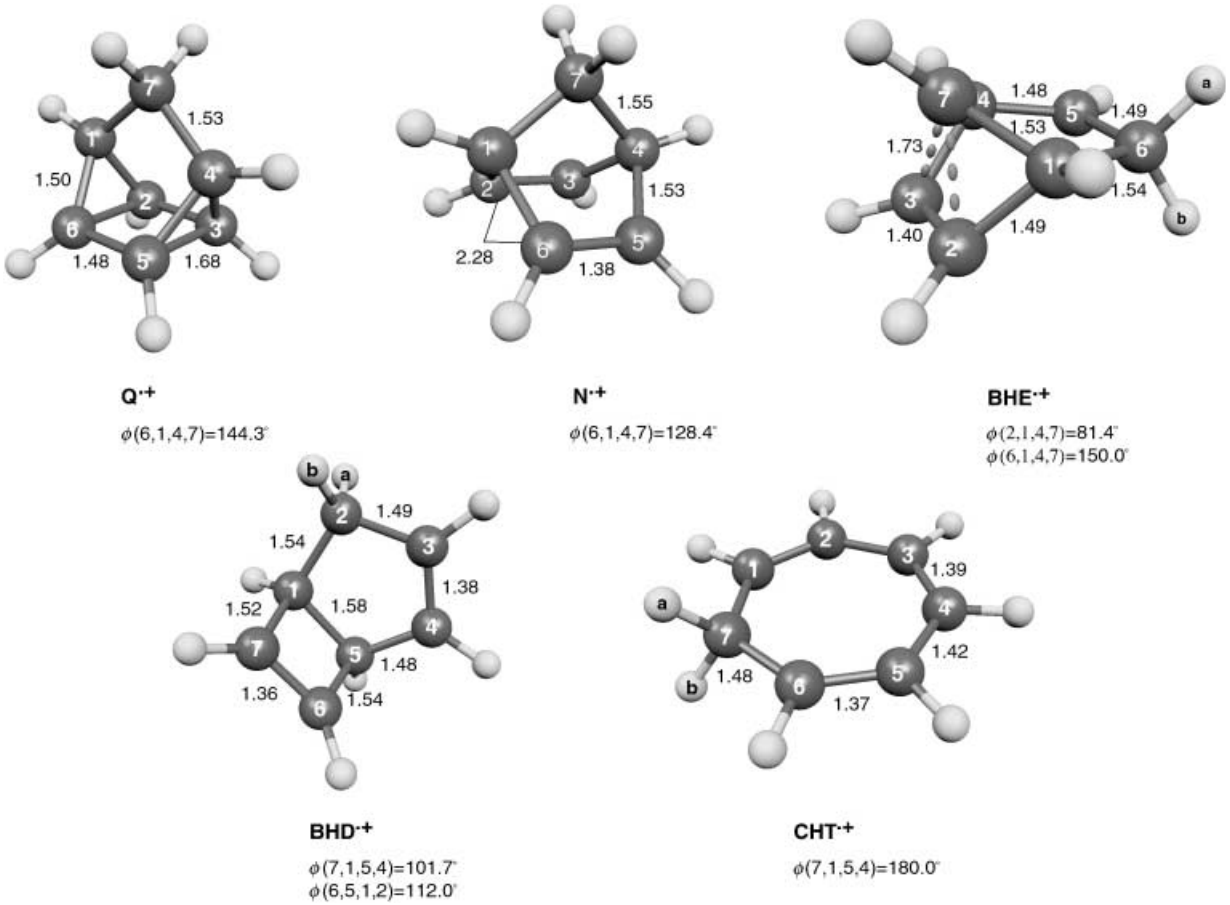

Figure 1. B3LYP/6–311+G(d,p) optimized stable structures of $C_7H_8^{\cdot+}$.

transition state, more ring opened; and for **TS6** (C2–C7 = 0.163 Å, C2-C1-C7 = 9.69°, and C2-C1-C6-C5 = 9.19°) MP2 again gives a more open structure. Since these parameters are involved in the reaction path they will affect our later analysis and calculation of activation barriers. For the continuing analysis we will mainly use the B3LYP optimized stationary points and their frequencies, since many of the MP2 results are too spin contaminated to be regarded as reliable. The other stationary points in Figures 2 and 3 have differences that are less than 0.068 Å for distances, 5.63° for angles, and 4.92° for dihedral angles.

Quadricyclane rearrangements: An energy profile for the activation energies at 100 K for the cycloreversion (**Q**$^{\cdot+}$, **TS1**, **N**$^{\cdot+}$) and the skeletal rearrangement (**Q**$^{\cdot+}$, **TS2**, **BHE**$^{\cdot+}$) is shown in Figure 4. This relative energy profile contains the zero-point energy correction and the free-energy thermal correction calculated from the B3LYP/6–311+G(d,p) frequencies, and the electronic energy taken from CCSD(T)/6–311+G(d,p)//B3LYP/6–311+G(d,p) calculations.

Calculations for the cycloreversion reaction path have been reported previously at several theoretical levels, including B3LYP with both the 6–31G* and 6–311+G(d,p) basis sets.[6,12] As we have reported earlier, the geometries of **TS1** agree well between these different theoretical levels, and show a pseudo-Jahn–Teller distorted transition structure with elongated C2–C6 and C3–C5 bonds in the four-membered ring,[12] but the relative electronic energies have larger variations (see Table 2 for some examples). Our best estimate for the activation free energy for the cycloreversion

Table 2. Relative electronic energies in kcal mol^{-1} for all located stationary points on the reaction paths investigated: first, the electrocyclic isomerization of **Q**$^{\cdot+}$ to **N**$^{\cdot+}$; and second, the rearrangements from **Q**$^{\cdot+}$ to **CHT**$^{\cdot+}$.

	B3LYP[a]	CCSD(T)//B3LYP[a]	UMP2[a]	PMP2[a]
Q$^{\cdot+}$	0.00	0.00	0.00	0.00
N$^{\cdot+}$	−10.73	−8.25	−6.15	−5.64
BHE$^{\cdot+}$	4.16	3.67	5.58	5.55
BHD$^{\cdot+}$	−1.84	6.18	14.65	11.33
CHT$^{\cdot+}$	−39.62	−22.49	−6.86	−13.76
TS1	12.08	11.63	15.48	13.73
TS2	13.41	16.49	21.70	20.24
TS3	9.51	11.72	17.74	14.49
TS4	18.49	21.96	33.39[b]	29.48[b]
TS5	12.19	21.96	27.94	26.72
TS6	9.80	12.49	17.63	14.75
I1	4.21	11.30	15.98	13.81
TS7	8.58	18.53	27.93	23.66
TS8	22.10	28.58	36.25	35.19
I2	3.79	13.15	20.08	19.09
TS9	7.58	17.82	23.17	22.85

[a] The energies are computed with B3LYP/6–311+G(d,p), CCSD(T)/6–311+G(d,p)//B3LYP/6–311+G(d,p), UMP2/6–311+G(d,p), and projected MP2 (PMP2/6–311+G(d,p)). [b] Energies taken from an U(P)MP2/6–311+G(d,p)//B3LYP/6–311+G(d,p) calculation.

 © 2004 Wiley-VCH Verlag GmbH & Co. KGaA, Weinheim

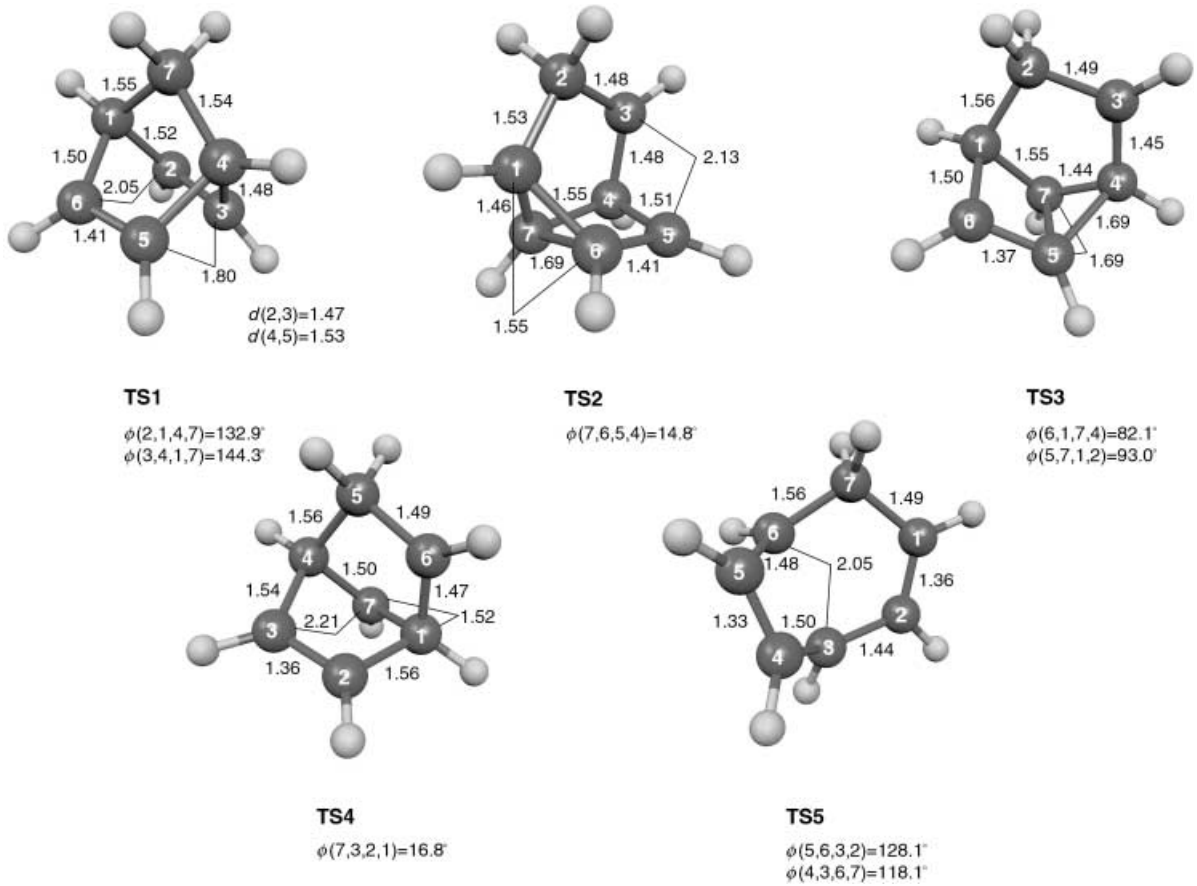

Figure 2. B3LYP/6–311+G(d,p) optimized transition structures for the cycloreversion (**TS1**), skeletal (**TS2**), stepwise (**TS3** and **TS5**), and concerted (**TS4**) rearrangements.

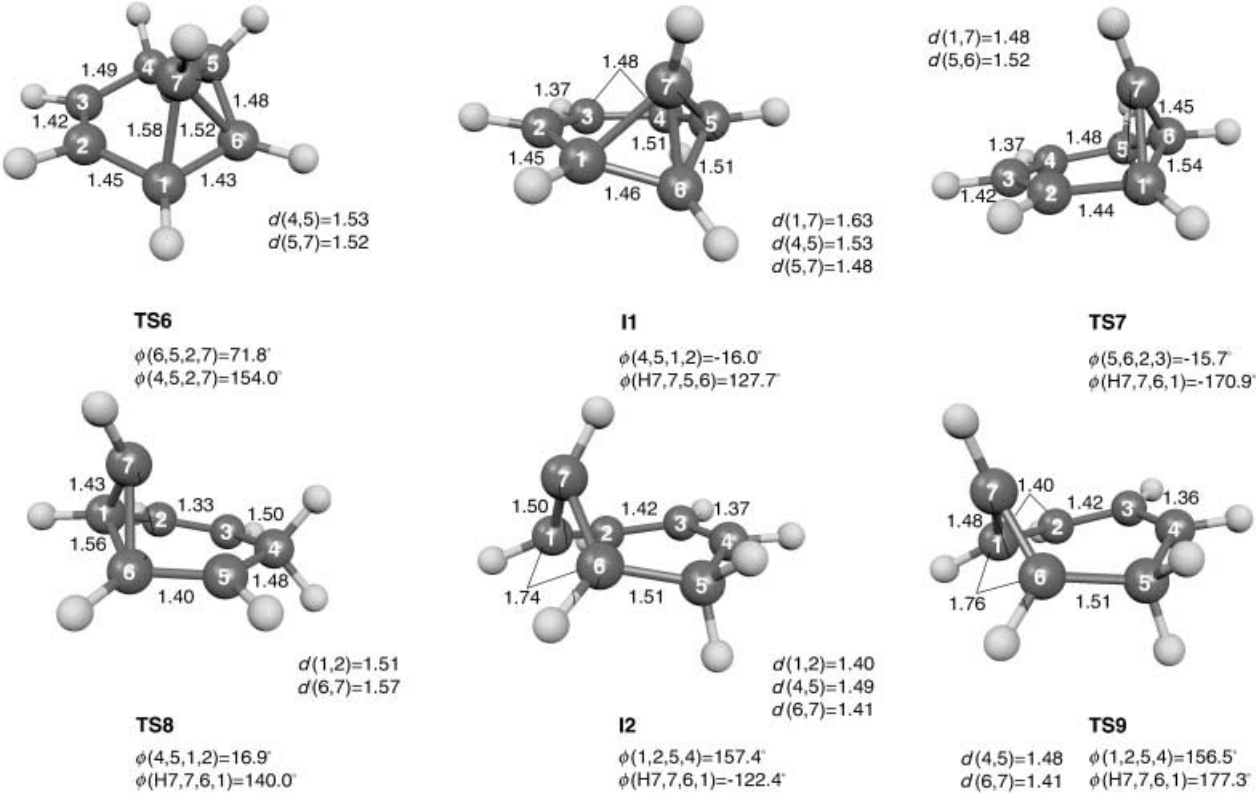

Figure 3. B3LYP/6–311+G(d,p) optimized stationary points for the multistep rearrangement.

© 2004 Wiley-VCH Verlag GmbH & Co. KGaA, Weinheim

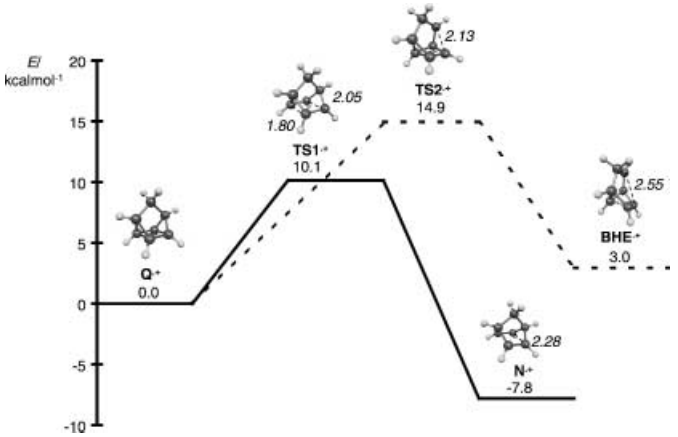

Figure 4. Free-energy profiles for the two $\mathbf{Q}^{\cdot+}$ isomerizations, a cycloreversion (**TS1**) to $\mathbf{N}^{\cdot+}$ and a skeletal rearrangement (**TS2**) to $\mathbf{BHE}^{\cdot+}$ in kcal mol^{-1}.

becomes 10.1 kcal mol^{-1} (cf. Table 3), agreeing well with the earlier estimations of theoretical activation energies in the range 5–12 kcal mol^{-1},[6] and the experimental estimation of 9.3 kcal mol^{-1}.[11]

The skeletal rearrangement to $\mathbf{BHE}^{\cdot+}$ has a transition state (**TS2**) in which one of the four lateral bonds (C1–C6, C1–C7, C3–C4, C3–C5) in the cyclopropane units in $\mathbf{Q}^{\cdot+}$ has opened. Breaking this bond costs more energy than for the pericyclic cycloreversion, since the estimated free energy of activation is 14.9 kcal mol^{-1}, see Table 3 and Figure 4. Hence, the skeletal rearrangement has 4.8 kcal mol^{-1} higher activation energy than the cycloreversion.

Table 3. Zero-point vibrational energies and free energies in kcal mol^{-1} for the stationary points on the investigated reaction paths.

	ZPVE	E_{rel}[a]	G_{rel}[b]
$\mathbf{Q}^{\cdot+}$	79.63	0.00	0.00
$\mathbf{N}^{\cdot+}$	80.11	−7.78	−7.79
$\mathbf{BHE}^{\cdot+}$	78.94	2.98	2.95
$\mathbf{BHD}^{\cdot+}$	78.44	4.99	4.93
$\mathbf{CHT}^{\cdot+}$	79.83	−22.29	−22.47
TS1	78.16	10.15	10.13
TS2	78.10	14.95	14.94
TS3	78.12	10.21	10.18
TS4	77.67	20.00	19.96
TS5	77.09	19.41	19.32
TS6	77.69	11.53	11.50
I1	78.59	10.26	10.21
TS7	77.69	16.58	16.52
TS8	77.00	25.95	25.88
I2	78.09	11.60	11.52
TS9	76.81	15.00	14.89

[a] The E_{rel} values include unscaled zero-point vibrational energy corrections taken from a B3LYP/6–311+G(d,p) calculation, and electronic energy from a CCSD(T)/6–311+G(d,p)//B3LYP/6–311+G(d,p) calculation. [b] The G_{rel} values include the free-energy thermal correction calculated at 100 K from unscaled B3LYP/6–311+G(d,p) vibrational frequencies.

Multistep rearrangement: The multistep rearrangement transforms $\mathbf{BHE}^{\cdot+}$ into $\mathbf{CHT}^{\cdot+}$ through two routes: $\mathbf{BHE}^{\cdot+}$ →**TS6**→**I1**→**TS7**→**I2**→**TS9**→$\mathbf{CHT}^{\cdot+}$ and $\mathbf{BHE}^{\cdot+}$ →**TS6**→**I1**→**TS8**→$\mathbf{CHT}^{\cdot+}$, for which the B3LYP/6–311+G(d,p) stationary points are shown in Figure 3. In addition, Figure 5 displays the free-energy profile at 100 K for this multistep rearrangement together with the two other possible isomerization reaction paths that $\mathbf{BHE}^{\cdot+}$ can take (see later). It

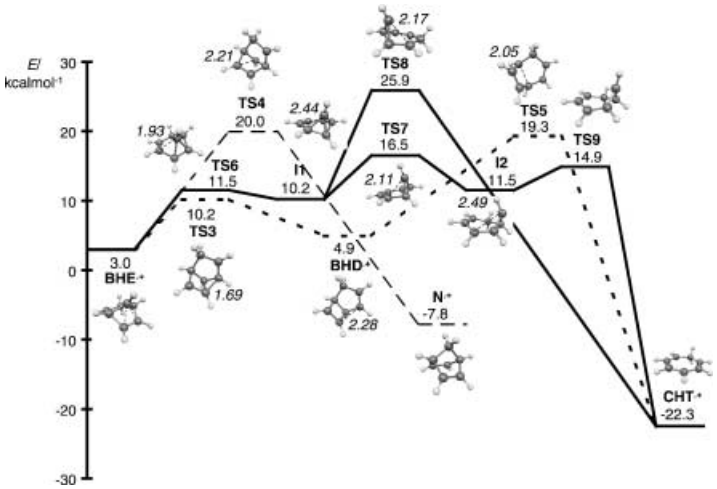

Figure 5. Comparison of the multistep, stepwise and concerted rearrangement free-energy profiles in kcal mol^{-1}.

should be noted that the most favorable energy profile is for the multistep rearrangement path passing through the rate-limiting step **TS7**, with an activation barrier of 16.5 kcal mol^{-1} above $\mathbf{Q}^{\cdot+}$.

The first step in this rearrangement is an almost complete bond breakage of the C4–C7 bond from 1.54 Å in $\mathbf{BHE}^{\cdot+}$ to 1.93 Å for the C2–C7 distance in **TS6**. At the same time, the three-center two-electron bond lengths (C2–C7 = 1.74 Å, C3–C7 = 1.73 Å) transform into distances in **TS6** that reflect more ordinary C–C single bonds (C1–C7 = 1.58 Å, C6–C7 = 1.52 Å). In the first intermediate, **I1**, this process has continued, and this distance (C2–C7 for **I1**) is 2.44 Å, but the C1–C7 bond also becomes elongated to 1.63 Å. This intermediate forms a very shallow minimum, with **TS6** being structurally similar to **I1**; there is only a 1.3 kcal mol^{-1} free energy barrier for the reversion to $\mathbf{BHE}^{\cdot+}$. The small imaginary frequency of −391.2 cm^{-1} for **TS6** and the lowest frequency for **I1** of 217.4 cm^{-1} both reflect the shallow well on the reaction path, since these normal modes closely mimic the reaction path.

From **I1** this isomerization path splits into two routes with transition states **TS7** and **TS8**; these routes both have a similar mechanism, but break bonds on opposite sides. In **TS7**, the C1–C7 bond of **I1** is opened to 2.11 Å, and in **TS8** the C5–C7 bond of **I1** is opened to 2.17 Å. Although the major coordinates involved in the respective mechanisms show strong similarities, the difference in reaction barrier of 9.36 kcal mol^{-1} (see Figure 5 and Table 3) implies that the differences in mechanism give rise to a large energy difference. For instance, the C1–C7 bond in **I1** is elongated relative to the normal C–C single bond length in the C5–C7 bond, and between **I1** and **TS8** the six-membered ring has to invert; this is reflected in $\phi(4,5,1,2) = -16.0°$ for **I1** and

 © 2004 Wiley-VCH Verlag GmbH & Co. KGaA, Weinheim

$\phi(4,5,1,2) = 16.9°$ for **TS8**. Both **TS7** and **TS8** have small imaginary frequencies, $-309.9\ cm^{-1}$ and $-259.5\ cm^{-1}$, with normal modes that closely follow the reaction coordinates.

The **TS8** route leads directly to **CHT$^{\cdot+}$**, while the **TS7** route isomerizes to another shallow intermediate, **I2**. The distance for the bond broken from **I1** to **TS7** becomes even longer, 2.49 Å; this is due to the rearrangement of the carbon skeleton and a partly broken C1–C6 bond. Thus, in **I2** the six-membered ring is slightly folded, $\phi(1,2,5,4) = 157.4°$, and the C1–C6 bond is opened to 1.74 Å. Moreover, **I2** has several very low vibrational frequencies (180.8, 223.8, 319.9, and $378.2\ cm^{-1}$) and their corresponding normal modes indicate that the floppy directions include both carbon skeletal motions and H7 motions.

The last step in this rearrangement is the complete opening of the C1–C6 bond and flattening of the carbon framework into the **CHT$^{\cdot+}$** C_{2v} geometry. In this mechanistic step **TS9** is a very early transition state. The dominating change on the reaction path up to **TS9** is a hybridization change of C7 from being pyramidalized in **I2** to sp^2 in **TS9**. This is, furthermore, reflected in the normal mode with imaginary frequency ($-607.7\ cm^{-1}$), which has a dominating contribution for this pyramidalization movement and a very minor component of opening and flattening of the carbon skeleton.

Stepwise rearrangement through BHD$^{\cdot+}$ to CHT$^{\cdot+}$: The other conversion to **CHT$^{\cdot+}$** follows a stepwise rearrangement path that goes through **BHD$^{\cdot+}$**: **BHE$^{\cdot+}$**→**TS3**→**BHD$^{\cdot+}$**→**TS5**→**CHT$^{\cdot+}$**. The rate-limiting step in this isomerization is the electrocyclic ring opening of **BHD$^{\cdot+}$** that has a free-energy barrier of $19.3\ kcal\,mol^{-1}$ above **Q$^{\cdot+}$**; this is $2.8\ kcal\,mol^{-1}$ higher than the multistep path (see Figure 5). In the first step, the reaction path changes its character around **TS3**. Before the transition state, the main reaction coordinate is the formation of a cyclopropane unit of the atoms C3, C4, and C7 in **BHE$^{\cdot+}$**; after **TS3** the major reaction coordinate is the breaking of the C4–C5 bond (1.69 Å) in **TS3**, which increases to 2.28 Å in **BHD$^{\cdot+}$**. This implies an early transition structure in which most of the C4–C5 bond breaking takes place after **TS3**. For the MP2 optimized path a much later transition structure is found, suggesting that most of the bond breaking is complete. The imaginary frequency for **TS3** of $-405.2\ cm^{-1}$ corresponds to a normal mode that closely mimics the C4–C5 bond breaking process. Because of this variation in transition structure along a reaction path that is similar for both B3LYP and MP2, the activation energy estimate is probably too low. Yet, our prediction, based on the B3LYP geometries, gives a barrier that is $10.2\ kcal\,mol^{-1}$ above **Q$^{\cdot+}$**.

The transition state for the electrocyclic ring-opening step (**TS5**) again indicates a change in major reaction coordinate along the reaction path. On this reaction path it is first a breakage of the bridge bond, that is, the C1–C5 bond in **BHD$^{\cdot+}$** is 1.58 Å and gets elongated to 2.05 Å in **TS5**; thereafter the strain release flattens the structure into **CHT$^{\cdot+}$**. The normal mode of the imaginary frequency ($-332.3\ cm^{-1}$) shows a continued opening of the C3–C6 distance. Also for this step there is a substantial difference between B3LYP and MP2 in the localization of the transition structure along the reaction path, but here MP2 predicts a less complete ring opening (1.75 Å); therefore, this again should result in an underestimated barrier height.

Since **BHE$^{\cdot+}$** is $2.0\ kcal\,mol^{-1}$ more stable than **BHD$^{\cdot+}$**, and the computed barrier for isomerization of **BHD$^{\cdot+}$** to **BHE$^{\cdot+}$** is $5.3\ kcal\,mol^{-1}$, which should be compared to the electrocyclic ring opening that has a barrier of $14.4\ kcal\,mol^{-1}$, it is plausible that **BHE$^{\cdot+}$** is found in experiments starting from **BHD$^{\cdot+}$**.[13] The fact that the calculated **BHE$^{\cdot+}$** hfcc values agree well with those from ESR measurements on irradiated **BHD** is, therefore, entirely consistent with the expectations from our calculations. Yet, if our predictions are correct, the stability of **BHD$^{\cdot+}$** indicates that it may be possible to experimentally characterize this radical cation intermediate.

Concerted rearrangement to N$^{\cdot+}$: The third reaction path from **BHE$^{\cdot+}$** is a concerted path to **N$^{\cdot+}$**. This reaction path (**BHE$^{\cdot+}$**→**TS4**→**N$^{\cdot+}$**) has an activation energy of 20.0 kcal mol^{-1} above **Q$^{\cdot+}$**, which is $3.4\ kcal\,mol^{-1}$ higher than the multistep rearrangement and $0.6\ kcal\,mol^{-1}$ higher than the stepwise rearrangement (see Figure 5). The geometric conversion that this reaction path follows is complex. Before the transition state (**TS4**) the three-center two-electron bond is broken, that is, the C2–C7 distance in **BHE$^{\cdot+}$** elongates from 1.73 Å to 2.21 in **TS4**. After **TS4**, a C2–C6 bond begins to form and, somewhat delayed, the C1–C2 bond breaks until eventually **N$^{\cdot+}$** is formed. In the imaginary frequency of **TS4** ($-312.2\ cm^{-1}$) the major part of the normal mode reflects the closing of the C2–C6 bond and a minor part the closing of the three-center bond.

Comparison of rearrangements: The activation energies for all studied rearrangements are presented in Figures 4 and 5, and in Table 3. The calculated reaction paths and activation energies are compatible with the experimental findings that **CHT$^{\cdot+}$** can be found in studies of **Q$^{\cdot+}$** and **N$^{\cdot+}$**.[4,7–9] Since the estimated barrier difference is $4.8\ kcal\,mol^{-1}$, it is likely that the matrix used in the experiment stabilizes the skeletal rearrangement path to **BHE$^{\cdot+}$** over that of the cycloreversion.[4,7] Moreover, the continued rearrangement should predominately proceed through the multistep mechanism, which has an activation energy $2.8\ kcal\,mol^{-1}$ lower than the stepwise mechanism. Yet, the reversion to **Q$^{\cdot+}$** is 1.6 kcal mol^{-1} lower than this multistep mechanism; this indicates that most **BHE$^{\cdot+}$** formed should react to **Q$^{\cdot+}$** if not matrix or solution effects, or substituent changes affect the activation energies in a judicious direction for **BHE$^{\cdot+}$**.

Rearrangement energies: The activation energies presented in the discussion of rearrangement mechanisms represent the best available estimate, that is, zero-point energy correction and the free-energy thermal correction calculated from B3LYP/6–311+G(d,p) frequencies, and the electronic energy taken from CCSD(T)/6–311+G(d,p)//B3LYP/6–311+G(d,p) calculations. In Table 2, relative electronic energies are reported for the B3LYP/6–311+G(d,p), CCSD(T)/6–311+G(d,p)//B3LYP/6–311+G(d,p), UMP2/6–311+G(d,p) and PMP2/6–311+G(d,p) methods. From this

© 2004 Wiley-VCH Verlag GmbH & Co. KGaA, Weinheim

table it can be noted that the relative energies show large discrepancies depending on the quantum chemical method used. In general, reaction barriers are bracketed by B3LYP, which has the lowest, and UMP2, with the highest calculated barriers; the smallest difference of ~3 kcal mol^{-1} found for **TS1** and the largest one of ~19 kcal mol^{-1} for **TS7**. CCSD(T) and PMP2 are in between with the CCSD(T) barrier being lower than PMP2. The large difference for **TS7** is probably due to a severely spin contaminated UMP2 wave function, since the PMP2 relative energy is ~4 kcal mol^{-1} lower than the UMP2. The CCSD(T) energy is ~10 kcal mol^{-1} higher than the B3LYP result, which indicates that the B3LYP barrier probably is underestimated. This may be the reason for the change in rate-limiting step for the multistep rearrangement, because B3LYP predicts **TS6** to be rate-limiting while CCSD(T), UMP2 and PMP2 predict **TS7**.

The local minima have the same type of bracketing, but with two exceptions. First, **N**$^{\cdot+}$ is predicted to be less stable with PMP2 than with UMP2, which is due to a more spin contaminated **Q**$^{\cdot+}$, that is, by projection the PMP2 energy is lowered more in **Q**$^{\cdot+}$ than in **N**$^{\cdot+}$. Second, for **BHE**$^{\cdot+}$ CCSD(T) gives the lowest relative energy, but it is only ~0.5 kcal mol^{-1} and ~2 kcal mol^{-1} lower than B3LYP and UMP2, respectively. In general, B3LYP seems to overestimate the stability of the local minima, with the important exception of **BHE**$^{\cdot+}$, for which all methods give similar energies. Moreover, the largest discrepancy is found in **CHT**$^{\cdot+}$, for which the relative energy differs by ~33 kcal mol^{-1}. This discrepancy is probably due to a combination of spin contamination and an overestimated stability in the B3LYP calculation.

Hence, B3LYP/6–311+(d,p), relative to CCSD(T), shows an imbalanced description of relative energies that gives the wrong ordering of stability for **BHD**$^{\cdot+}$ and **BHE**$^{\cdot+}$, predicts **CHT**$^{\cdot+}$ to be ~17 kcal mol^{-1} more stable, and gives an activation energy that is ~10 kcal mol^{-1} lower than the CCSD(T) result for the multistep mechanism. With such large discrepancies in relative energies it may be necessary to explore if other functionals could give better agreement with high-level ab initio energetics and achieve the same accuracy of hfcc in radical cation studies.

Conclusion

In conclusion, we have located two plausible reaction paths that show how **CHT**$^{\cdot+}$ can be formed from **Q**$^{\cdot+}$, see Figures 4 and 5. The most advantageous is the multistep rearrangement that has a rate-limiting step with an estimated activation energy of 16.5 kcal mol^{-1}, which is 2.8 kcal mol^{-1} lower than for the stepwise mechanism. Yet, the lowest activation energy is found for the reverse skeletal rearrangement to form **Q**$^{\cdot+}$, which is 1.6 kcal mol^{-1} lower than the multistep mechanism. For the two **Q**$^{\cdot+}$ rearrangements, the cycloreversion path has a transition structure that is in close correspondence with earlier studies and an estimated activation energy of 10.1 kcal mol^{-1}, which agrees well with the experimental estimate of 9.3 kcal mol^{-1}.[3] The activation energy of 14.9 kcal mol^{-1} for the skeletal rearrangement is plausible, recalling that at no time in the zeolite study the conversion rate is higher than 3%.[4]

Computational Methods

All calculations were performed with Gaussian 98,[15] and the abbreviations used throughout this paper are taken from this program package. First a preliminary investigation of the $C_7H_8^{\cdot+}$ potential-energy surface was carried out with the B3LYP functional[16] with the 6–31G(d) basis set. In this first step we located and optimized all minima and transition states. This was done with the standard algorithm in Gaussian for optimization, and with the synchronous transit-guided quasi-Newton method,[17] which we used to force a mapping of more directions on the potential-energy surface than those directly obvious from the optimized minima. All stationary points were characterized to have the correct type of vibrational eigenvalues, and saddle points were verified to connect to the correct minima by means of a combination of the internal reaction coordinate (IRC) method,[18] around the transition state region, and then a steepest descent optimization for continuing the reaction path to the minimum. In a second step, the stationary points located with B3LYP/6–31G(d) were reoptimized with both B3LYP/6–311+G(d,p) and MP2/6–311+G(d,p), and characterized as minima or transition structures. This extra confirmation of the optimized structures was carried out because we noticed that B3LYP3–21G gives spurious structures and energetics for the **BHE**$^{\cdot+}$ and **BHD**$^{\cdot+}$ minima, which are artifacts of this small basis set. In hydrocarbon ring-systems it is necessary to use basis sets that include polarization functions to get a reliable description.[19] Finally, the B3LYP/6–311+G(d,p) geometries were used in coupled cluster single-point calculations of the energy including singles, doubles, and perturbative triples (CCSD(T)/6–311+G(d,p)); the zero-point vibrational energy and the free-energy correction at 100 K were taken from unscaled B3LYP/6–311+G(d,p) frequencies. All molecular pictures, and visualization of vibrational modes, were constructed with Molekel.[20]

The stationary point wavefunctions were checked for spin contamination by evaluation of the spin operator expectation value, $\langle S^2\rangle$. A pure doublet has $\langle S^2\rangle = 0.75$. Before spin projection all B3LYP results had $\langle S^2\rangle$ ranging between 0.75 and 0.77. The UHF reference wave functions used for the MP2 stationary points were in general found to be more spin contaminated, $\langle S^2\rangle = 0.76$–1.02. Moreover, the MP2 computed transition structures were more contaminated ($\langle S^2\rangle = 0.77$–0.91) than **N**$^{\cdot+}$, **Q**$^{\cdot+}$ and **BHE**$^{\cdot+}$ (0.76, 0.77, 0.77); while **BHD**$^{\cdot+}$, **CHT**$^{\cdot+}$, **I1** and **I2** were as contaminated or more (with $\langle S^2\rangle = 0.88$, 1.02, 0.83 and 0.81). By spin projection the MP2 wave functions were improved, $\langle S^2\rangle = 0.75$–0.79, for all stationary points. In the CCSD(T)/6–311+G(d,p) calculations the spin contamination was a less severe problem, since the principal spin contaminant is annihilated from the CCSD wavefunction.[21]

Acknowledgment

We thank the Swedish National Supercomputer Center (NSC) for generous allocation of computer time.

[1] M. Schmittel, A. Burghart, *Angew. Chem.* **1997**, *109*, 2659–2699; *Angew. Chem. Int. Ed. Engl.* **1997**, *36*, 2550–2589.
[2] P. G. Gassman, J. W. Hershberger, *J. Org. Chem.* **1987**, *52*, 1337–1339.
[3] K. Ishiguro, I. V. Khudyakov, P. F. McGarry, N. F. Turro, H. D. Roth, *J. Am. Chem. Soc.* **1994**, *116*, 6933–6934.
[4] K. R. Cromack, D. W. Werst, M. V. Barnabas, A. D. Trifunac, *Chem. Phys. Lett.* **1994**, *218*, 485–491.
[5] H. D. Roth, M. L. Manion Schilling, G. Jones, *J. Am. Chem. Soc.* **1981**, *103*, 1246–1248.
[6] a) T. Clark, *Acta Chem. Scand.* **1997**, *51*, 646–652; b) Y. Inadomi, K. Morihashi, O. Kikuchi, *J. Mol. Struct.* **1998**, *434*, 59–66; c) R. D. Bach, I. L. Schilke, H. B. Schlegel, *J. Org. Chem.* **1996**, *61*, 4845–

 © 2004 Wiley-VCH Verlag GmbH & Co. KGaA, Weinheim

4847; d) K. Raghavachari, R. C. Haddon, H. D. Roth, *J. Am. Chem. Soc.* **1983**, *105*, 3110–3114.
[7] G.-F. Chen, J. T. Wang, F. Williams, K. D. Belfield, J. E. Baldwin, *J. Am. Chem. Soc.* **1991**, *113*, 9853–9855.
[8] M. V. Barnabas, D. W. Werst, A. D. Trifunac, *Chem. Phys. Lett.* **1993**, *206*, 21–24.
[9] R. E. Bühler, M. A. Quadir, *J Phys. Chem. A* **2000**, *104*, 2634–2640.
[10] W. Adam, T. Heidenfelder, C. Sahin, *J. Am. Chem. Soc.* **1995**, *117*, 9693–9698.
[11] R. Herges, F. Starck, T. Winkler, M. Schmittel, *Chem. Eur. J.* **1999**, *5*, 2965–2970.
[12] a) P.-E. Larsson, N. Salhi-Benachenhou, X. Dong, S. Lunell, *Int. J. Quantum Chem.* **2002**, *90*, 1388–1395; b) P.-E. Larsson, N. Salhi-Benachenhou, S. Lunell, *Org. Lett.* **2003**, *5*, 1329–1331.
[13] A. Faucitano, A. Buttafava, F. Martinotti, R. Sustmann, *J. Chem. Soc. Perkin Trans. 2* **1992**, 865.
[14] a) A. Faucitano, A. Buttafava, F. Martinotti, *Radiat. Phys. Chem.* **1995**, *45*, 45–49; b) K. R. Cromack, D. W. Werst, E. E. Tartakovsky, A. D. Trifunac, *Chem. Phys. Lett.* **1994**, *229*, 421–428.
[15] Gaussian 98 (Revision A.7), M. J. Frisch, G. W. Trucks, H. B. Schlegel, G. E. Scuseria, M. A. Robb, J. R. Cheeseman, V. G. Zakrzewski, J. A. Montgomery, R. E. Stratmann, J. C. Burant, S. Dapprich, J. M. Millam, A. D. Daniels, K. N. Kudin, M. C. Strain, O. Farkas, J. Tomasi, V. Barone, M. Cossi, R. Cammi, B. Mennucci, C. Pomelli, C. Adamo, S. Clifford, J. Ochterski, G. A. Petersson, P. Y. Ayala, Q. Cui, K. Morokuma, D. K. Malick, A. D. Rabuck, K. Raghavachari, J. B. Foresman, J. Cioslowski, J. V. Ortiz, A. G Baboul, B. B. Stefanov, G. Liu, A. Liashenko, P. Piskorz, I. Komaromi, R. Gomperts, R. L. Martin, D. J. Fox, T. Keith, M. A. Al-Laham, C. Y. Peng, A. Nanayakkara, C. Gonzalez, M. Challacombe, P. M. W. Gill, B. G. Johnson, W. Chen, M. W. Wong, J. L. Andres, M. Head-Gordon, E. S. Replogle, J. A. Pople, Gaussian, Inc., Pittsburgh, PA, **1998**.
[16] a) C. Lee, W. Yang, R. G. Parr, *Phys. Rev.* **1988**, *37*, 785; b) A. D. Becke, *J. Chem. Phys.* **1993**, *98*, 5648; c) P. J. Stephens, F. J. Devlin, C. F. Chablowski, M. J. Frisch, *J. Phys. Chem.* **1994**, *98*, 11623.
[17] P. Y. Ayala, H. B. Schlegel, *J. Chem. Phys.* **1997**, *107*, 375–384.
[18] C. Gonzalez, H. B. Schlegel, *J. Chem. Phys.* **1989**, *90*, 2154–2161.
[19] P. C. Hariharan, J. A. Pople, *Chem. Phys. Lett.* **1972**, *16*, 217.
[20] P. Flükiger, H. P. Lüthi, S. Portmann, J. Weber MOLEKEL 4.1; Swiss Center for Scientific Computing, Manno (Switzerland), 2000–2001.
[21] H. B. Schlegel, *J. Phys. Chem.* **1988**, *92*, 3075.

Received: April 23, 2003
Revised: September 8, 2003 [F5067]

© 2004 Wiley-VCH Verlag GmbH & Co. KGaA, Weinheim